Received: 14 September 2020 | Revised: 24 November 2020 | Accepted: 17 January 2021

DOI: 10.1002/we.2624

RESEARCH ARTICLE

Performance of an omnidirectional piezoelectric wind energy harvester

Tianyi Shi[1] | **Gang Hu**[2] | **Lianghao Zou**[1] | **Jie Song**[1,3] | **Kenny C.S. Kwok**[4]

[1] Engineering Research Center of Urban Disasters Prevention and Fire Rescue Technology of Hubei Province, School of Civil Engineering, Wuhan University, Wuhan, China

[2] School of Civil and Environmental Engineering, Harbin Institute of Technology, Shenzhen, China

[3] Department of Civil & Mineral Engineering, University of Toronto, Toronto, Ontario, Canada

[4] Centre for Wind, Waves and Water, School of Civil Engineering, The University of Sydney, Sydney, New South Wales, Australia

Correspondence
Lianghao Zou and Jie Song, Engineering Research Center of Urban Disasters Prevention and Fire Rescue Technology of Hubei Province, School of Civil Engineering, Wuhan University, Wuhan, China.
Email: lhzou@whu.edu.cn; songjie@whu.edu.cn

Funding information
Shenzhen Basic Research Program, Grant/Award Number: JCYJ20170811160652645; National Natural Science Foundation of China, Grant/Award Numbers: 51478369, 51608398

Abstract

This paper presents a vortex-induced vibration (VIV)-based piezoelectric energy harvester that performs well for all wind directions, a so-called omnidirectional wind energy harvester. The kinetic energy of this harvester stems from wind-induced vibrations of a circular cylinder mounted on an orthogonal bibeam system, rather than a traditional single beam. Wind tunnel testing results show that compared to the traditional single-beam energy harvester, the proposed harvester substantially enhances the effectiveness, in most cases that the beam is skew to the incoming flow. The reasons for the enhancement are explained in detail by examining the wind-induced displacement response components of the cylinder identified by the image processing technique. For all wind directions, both the maximal output energy and the range of effectively working wind speed of the proposed bibeam wind energy harvester are significantly improved with respect to the single-beam system, indicating excellent performance of the proposed omnidirectional harvester in a natural wind environment.

KEYWORDS

omnidirectional wind energy harvester, piezoelectricity, two degree-of-freedom, vortex-induced vibration (VIV)

1 | INTRODUCTION

Piezoelectric energy harvesters (EHs) have attracted substantial attention in the last decades. EHs can generate sustainable power and hence are promising as an alternative to batteries that have a limited life span while require costly maintenance.[1,2] Piezoelectric EHs, therefore, can be an excellent power source for self-powered devices such as microelectromechanical systems (MEMS) and wireless sensor networks (WSNs). Among different vibration-based energy resources, wind flow has been suggested as one of the most reliable energy resources, since wind-induced vibrations of bluff bodies could have considerable amplitudes even when subjected to low-speed wind.[3,4] Consequently, piezoelectric EHs based on wind-induced vibrations of bluff bodies are able to produce considerable electric energy. Wind-induced vibrations commonly utilized in piezoelectric wind EHs include vortex-induced vibration (VIV),[5,6] galloping,[7–10] flutter,[11–13] and mixed aerodynamic phenomena.[14–16] Several comprehensive reviews on harnessing energy from wind flow have been published recently.[17–22]

The VIV is usually considered as an undesirable phenomenon in engineering practice, as it may cause tremendous damage to buildings, chimney, offshore structures, and cables.[23–25] On the other hand, the vibration can also be used to generate electric energy using piezoelectric devices. Bernitsas et al.[26] proposed a device called Vortex-Induced Vibration Aquatic Clean Energy (VIVACE) that used the oscillations induced by the vortex shedding from a spring-mounted circular cylinder in a range of flow velocities to generate electricity. Akaydin et al.[27] examined a VIV piezoelectric EH that consisted of a cylinder attached to the free end of a piezoelectric cantilevered beam. The effects of the resonant frequency and structural damping on the performance of the harvester were evaluated. Meanwhile, the optimal wind speed and peak harvested power were determined in their research. Abdelkefi et al.[5] and Dai et al.[6] developed a lumped-parameter model and a nonlinear distributed parameter model, respectively. The effects of the electrical load resistance on the synchronization region and levels of the harvested power have been investigated in the two studies.

The VIV-based wind EHs have been improved substantially in the past few years. Various strategies have been proposed to broaden the range of working velocity and promote the efficiency of the harvester. These strategies include employing nonlinear forces, optimizing the aerodynamic shape, and utilizing different concurrent vibration sources. For instance, Mehmood et al.[28] investigated the harvested energy from the VIV by numerical simulations. Results showed that there was an optimum value of the electrical load resistance to acquire the maximum harnessed power. Abdelkefi et al.[29] and Zhang et al.[30] investigated the interference of dual tandem circular cylinders to improve the output performance of the harvester. Their results showed that the harnessed power was greatly enhanced and the bandwidth of the resonance region was also increased, compared to that of the original single EH. Zhang et al.[31] proposed a VIV-based wind EH by introducing nonlinear magnet forces, which showed a wider resonance/synchronization region and a higher level of the harvested power than those of the traditional configuration. From a theoretic point of view, Naseer et al.[32] designed a monostable ultrawide bandwidth VIV-based piezoelectric wind EH by employing nonlinear magnetic forces. Their harvester can enhance the performance of EH when the ambient wind condition is not ideal. Song et al.[33] examined the effect of the splitter plate placed in the near wake of a circular cylinder on the performance of a piezoelectric wind EH. The results showed that the harvester was able to keep large amplitude vibrations even beyond the lock-in wind speed range and hence the range of effectively working wind speed was expanded. Hu et al.,[34,35] and Ding et al.[36] investigated the wind EH with two small-size rod-shaped attachments on the main circular cylinder. The harvester can harness the wind energy beyond the VIV onset wind speed too and still can work efficiently over the range of lock-in wind speed. Dai et al.[37] investigated a piezoelectric EH that harnessed the energy from both base excitation and VIV. Compared to the two harvesters that make use of each single excitation, their harvester showed a 50% increase in the harnessed power. Qin et al.[38] presented a wind EH with two square cylinders and a circular cylinder, which was able to harness energy from both the VIV and the galloping. Thus, their harvester kept a stable output power even when the wind speed varied in a wide range. Petrini and Gkoumas[14] focused on the conceptual development, analytical modeling, and wind tunnel testing of a high efficiency EH, which took advantages of VIV and galloping with circular and T-shape cross section. Shan et al.[15] presented a piezoelectric EH system for the concurrent flutter-induced vibration and VIV. The wind tunnel experiment results showed better output performance over the existing harvesters.

As discussed above, most of the previous studies focused on increasing the efficiency and/or broadening the range of working wind speed of wind EHs. Furthermore, the majority of the wind EHs have been tested for optimization design just in laboratories and hence are under ideal or specific wind conditions. As a result, discrepancies from the ideal or specific wind conditions, such as turbulence and change in wind direction, can influence the performance of the designed wind EHs potentially used in a natural wind environment. The turbulence affects the stability of VIV and causes buffeting. The turbulence intensity tends to decrease VIV amplitude of a smooth circular cylinder in the lock-in region.[39,40] One distinct characteristic of natural wind in reality is that the wind flow can come from any direction, rather than maintaining one direction only. Therefore, a few different strategies, for example, aerodynamic treatments of bluff body and optimization of structures, have been proposed to harness wind energy from multiple wind directions. Li et al.[41] designed a polymer piezoelectric EH with three distinct operation modes in three directions, which can generate energy for three wind directions. An EH with an arc-shaped elastic beam was designed to extract wind energy from three wind directions as well.[42] Although these harvesters can work efficiently in three particular wind directions, they still cannot be directly applied in practice because of the uncertainty of wind direction in reality.

In view of the above limitation, a rotational piezoelectric wind EH has been developed to work efficiently for all wind directions, by rotating the harvester against wind. For instance, appending a self-aligning device to the harvester was proved to have the ability to improve the performance of the harvester for different wind directions.[12] A direction-adaptive harvester with a guide vane was designed by Gong et al.[43] There results indicated that the harvester performed well when changing wind direction. However, the self-aligning device and the guide vane are space consuming and complex, which contradicts the microminiaturization of EHs and hence inhibits their practical application.

To overcome the limitation of the piezoelectric wind EHs on specific working wind directions and fulfill the practice need of all wind directions, this study develops a compact bibeam wind EH that can work effectively when wind flows from any directions, that is, an omnidirectional wind EH, but remaining a small volume. The configuration of the proposed bibeam wind EH is explained in detail, with the governing equation of motions of the system. A series of wind tunnel tests are carried out to examine the performance of the proposed bibeam wind EH. The performance of the bibeam wind EH is compared with that of the traditional single-beam wind EH, to validate advantages of the proposed wind EH for all wind directions. The vibration mechanism of the proposed bibeam wind EH is also explained by examining the wind-induced structural responses of the harvester. The key findings are summarized in the conclusion, which accelerate the development of the omnidirectional VIV-based piezoelectric wind EHs.

2 | PROPOSED OMNIDIRECTIONAL BIBEAM WIND EH

2.1 | Configuration of bibeam wind EH

A compact design of the bibeam wind EH, as shown in Figure 1A, is proposed to overcome the limitation on specific working wind directions of the majority of existing wind EHs. In other words, the harvester in the design is endowed with the capability of working efficiently in any wind direction and hence performs as an omnidirectional EH. As shown in Figure 1A, the proposed wind EH consists of a circular cylinder mounted on a bibeam with two piezoelectric sheets (PESs) in which the two subbeams are connected orthogonally, rather than on a single common beam. The associated traditional single-beam EH consisting of a circular cylinder and a normal single beam with a single PES is also shown in Figure 1B as a reference. As shown in Figure 1C, x and y directions are the along and across wind directions, respectively. The wind direction θ is the angle between x direction and v direction. Due to the structural and geometric symmetry, the proposed harvester can then regarded as a two degree-of-freedom (*dof*) system with a bibeam: one *dof* is the transverse vibration of the upper subbeam along direction u, and the other *dof* is the transverse vibration of the lower subbeam along direction v. In addition, the transverse vibration frequencies in these two directions are designed to be identical according to the classical cantilever beam theory, by changing the length of the lower beam and identifying the vibration frequency in each direction. In this way, the harvester is expected to be excited by wind flow from any direction. Two PESs are attached on each subbeam, respectively, to convert the vibrations to electrical energy, as shown in Figure 1D,E.

2.2 | Governing equations of the system

For better understanding of the performance of omnidirectional piezoelectric wind EH, the governing equations of the system shown in Figure 1A are given in this section. Considering the first mode in each direction, that is, the first two modes of the system, the governing equations of the proposed bibeam EH are written as

$$M_1\ddot{u} + C_1\dot{u} + K_1 u + \Theta_1 V_1(t) = F_{fluid,u}, \tag{1}$$

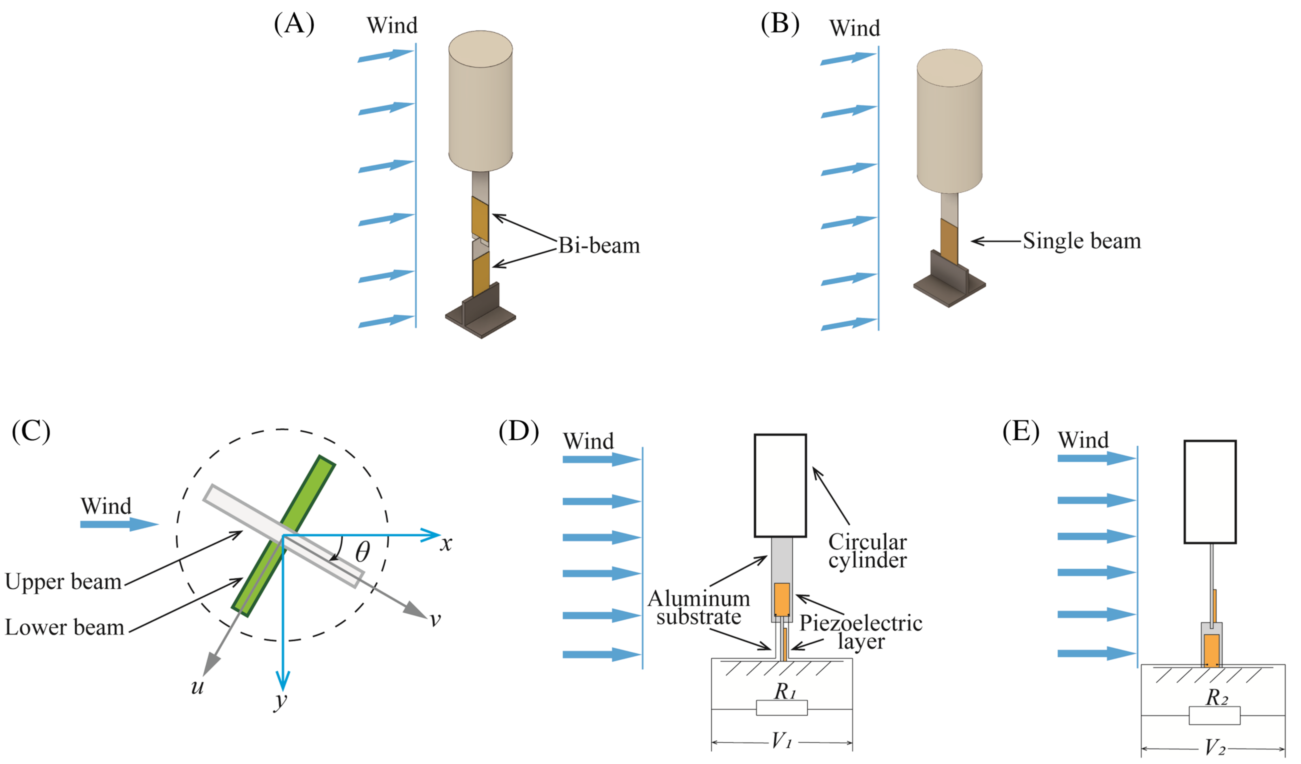

FIGURE 1 (A) Configuration of the proposed bibeam wind EH, (B) configuration of the traditional single-beam wind EH, (C) top view of the proposed bibeam wind EH, (D) lateral view of the proposed bibeam wind EH at $\theta = 0^\circ$, and (E) lateral view of the proposed bibeam wind EH at $\theta = 90^\circ$

$$C_{p1}\dot{V}_1 + \frac{V_1}{R_1} - \Theta_1\dot{u} = 0, \tag{2}$$

$$M_2\ddot{v} + C_2\dot{v} + K_2v + \Theta_2V_2(t) = F_{fluid,v}, \tag{3}$$

$$C_{p2}\dot{V}_2 + \frac{V_2}{R_2} - \Theta_2\dot{v} = 0, \tag{4}$$

where u and v are the displacement of cylinder in the direction corresponding to the first mode in each direction, as shown in Figure 1C; M_i (i = 1 or 2), C_i, and K_i are the generalized mass, damping, and stiffness, respectively, and the subscript i denotes the mode number; Θ_i, C_{pi}, V_i, and R_i are the electromechanical coupling term, the capacitance of the PES, the generated voltage, and the load resistance, respectively; and $F_{fluid,u}$ and $F_{fluid,v}$ are the components of vortex-induced force in u and v directions, respectively.

3 | WIND TUNNEL TESTS

The wind tunnel tests in this study have been conducted in the open-circuit wind tunnel at Wuhan University, as shown in Figure 2. The wind tunnel has a 40 cm × 40 cm test cross section and a low-turbulence flow with a turbulence intensity less than 1.5%. The length, width, and thickness of the upper aluminum cantilever beam are 7, 1.8, and 0.06 cm, respectively. The length, width, and thickness of the lower aluminum cantilever beam are 4.5, 1.8, and 0.07 cm, respectively. The circular cylinder is made of light foam with a length of 10 cm and a diameter D of 5 cm. The vibration frequencies f of the first and second modes, corresponding to the transverse vibrations of the upper beam (along u) and the lower beam (along v), respectively, are set to be identical to 14.1 Hz. As mentioned before, the symmetry of the bibeam wind EH enables that the vibrations in u and v directions are independent. The modes and frequencies are calculated by classical cantilever beam theory, and then, the two vibration frequencies are set to be identical by adjusting the length of the lower beam. The structural damping ratios of the first mode and second mode are 0.62% and 0.88% of the critical damping, respectively. The upper and lower PESs (MFC-2814P2, Smart Material Corp., C_p = 15.7 nF) are connected to the two electrical load resistances R_1 and R_2. The voltages V_1 (upper PES) and V_2 (lower PES) across the load resistances are measured by a DAQ module (NI-9229, National Instruments). The wind speed U of the incoming flow is measured by an anemometer (Testo 425, Testo SE & Co.). The displacement responses at the top of the circular cylinder subjected to wind flow with different mean wind speed are measured based on the image processing technique by using a high-speed camera (OSG030-815UC, YVsion Company) fixed above the harvester. The high-speed camera provides frame rates up to 815 frames per second. The image processing technique by Hough transform[44,45] is adopted in the

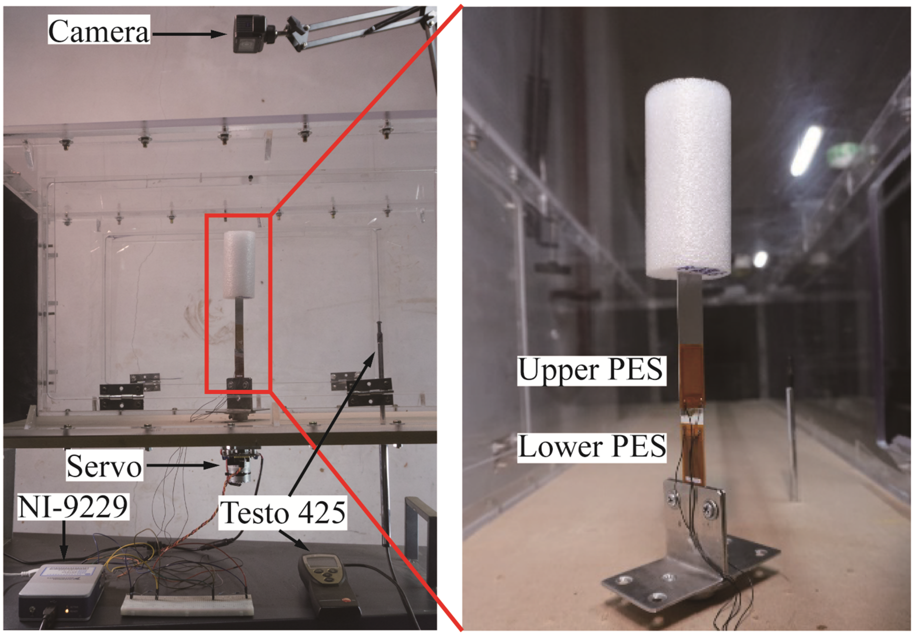

FIGURE 2 Configuration of the bibeam wind energy harvester in the wind tunnel

measurement of displacement responses. This is because the cylinder's excessive vibrations are hard to be measured by the laser displacement meter, whereas the responses can be measured by the image processing technique quickly and efficiently. The displacement responses of the single-beam wind EH measured by the image processing technique are compared with those measured by the traditional laser displacement meter (LK-G400, KEYENCE), as shown in Figure 3. As can be seen, the two curves are very close to each other, which verifies the high accuracy of the image processing technique. More importantly, the signal identified by the image processing technique is smoother than that measured by the laser displacement meter. Due to symmetry of the harvester, the tests are carried out only for a quadrant from wind direction $\theta = 0^\circ$ to 90° at 11.25° increments. The wind directions of $\theta = 0^\circ$ and 90° are parallel with directions v and u, respectively. For each wind direction θ, therefore, the vibrations in directions u and v and output voltages V_1 and V_2 are recorded for the subsequent analysis.

The time histories of the measured displacement responses at the cylinder's top and the two output voltages V_1 and V_2 from the two PESs are shown in Figure 4, for wind speed $U = 3.51$ m/s and wind direction $\theta = 0^\circ$. As can be seen from Figure 4, both the displacement responses and the output voltages are nearly perfect harmonic, due to the periodic VIVs of the cylinder. Furthermore, for $U = 3.51$ m/s and $\theta = 0^\circ$, the VIVs of the cylinder are dominant, and hence, the cross-wind responses in direction u are far larger than the along-wind responses in direction v. As a result, the output voltage V_1 caused by the vibrations of the upper beam along direction u is far more considerable than V_2 caused by the vibrations of the lower beam along direction v, which partly validates the reliability of the measurement system.

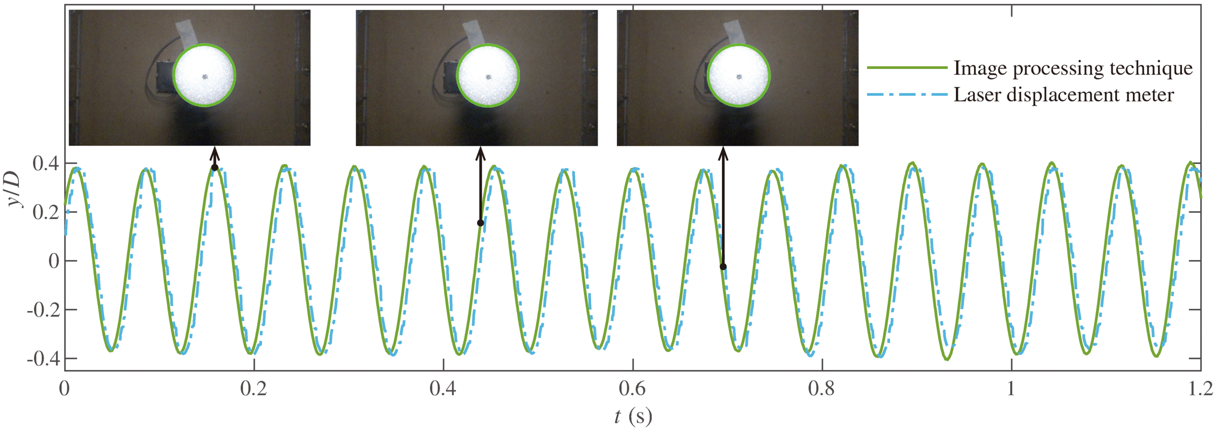

FIGURE 3 Comparison of the displacement responses measured by the image processing technique and the laser displacement meter

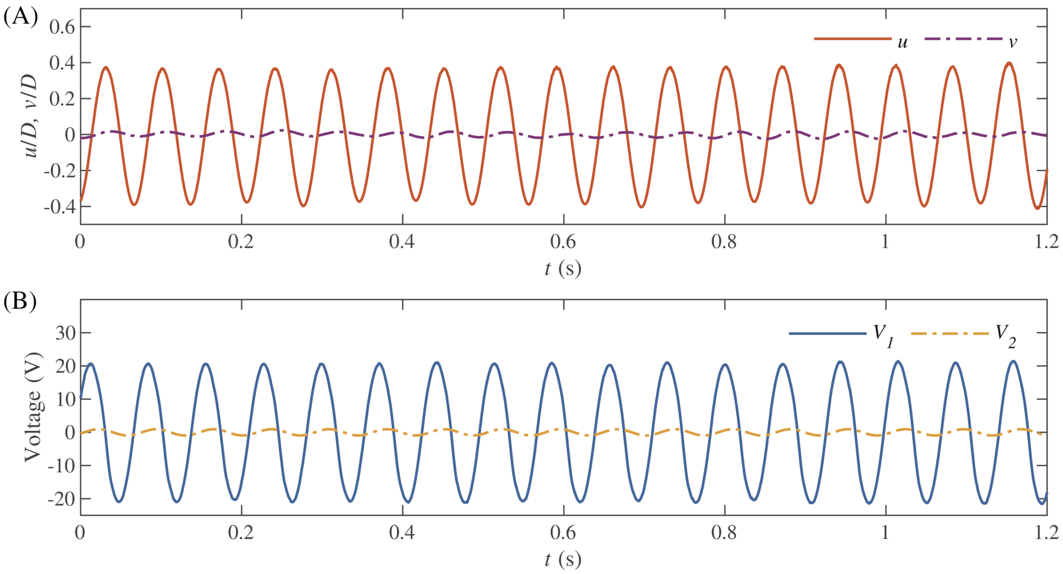

FIGURE 4 Time histories for $U = 3.51$ m/s and $\theta = 0$: (A) wind-induced displacement responses at the cylinder top and (B) output voltages of the two PESs

4 | PERFORMANCE OF THE PROPOSED OMNIDIRECTIONAL PIEZOELECTRIC WIND EH

4.1 | The optimal electrical load resistance

Since the performance of a piezoelectric wind EH varies with electrical load resistance, tuning electrical load resistance to realize the maximal harnessed power at the synchronization region is carried out before investigating the performance. The average output power of the bibeam wind EH is computed by the associated voltage as $P_i = V_{rms,i}{}^2/R_i$, where V_{rms} is the root mean square of voltage, $i = 1$ or 2, denoting the upper or lower PES. Figure 5 shows the variations of the average output power of the bibeam wind EH with electrical load resistance. As can be seen, P_1 and P_2 reach the maximum when $R_1 = R_2 = 4 \times 10^5$ Ω for wind direction 0° and 90°, respectively, at a wind speed $U = 3.51$ m/s. Therefore, $R_1 = R_2 = 4 \times 10^5$ Ω is the optimal electrical load resistance and is then used for the bibeam wind EHs in the subsequent tests and discussion.

4.2 | Performance of the traditional single-beam EH

For comparison, this section briefly examines the performance of the associated single-beam EH shown in Figure 1B. The single-beam EH has the same structural properties as those of the first mode of the proposed bibeam EH, to maintain consistency. The variation of the average output power of the single-beam EH with wind speed U and direction θ is shown in Figure 6. For wind direction $\theta = 0°$, the output power increases significantly when the reduced wind velocity U_r ($=U/fD$) exceeds 4 and decreases dramatically when $U_r > 8$. It is obvious that the output power when $4 < U_r < 8$ is considerable, because of the significant VIVs of the circular cylinder of the harvester. And this range of wind velocity with a large output power is associated with the critical reduced wind speed U_c of the circular cylinder ($U_c \approx 5$, as Strouhal number for a circular cylinder[46,47] is around 0.2). This range is also the lock-in/synchronization region that enables the VIV-based wind EH to operate in a wide range of wind velocity. When θ becomes 22.5°, the maximum output power decreases to 1.8 mW. In addition, the lock-in region for $\theta = 22.5°$ is narrower than that for $\theta = 0°$. This because when $\theta = 22.5°$, the direction of vibration deviates from the cross-wind direction, and hence, the component of the cross-wind force $F_{fluid,u}$ along the direction of vibration is decreased. As a result, the vibration amplitude for $\theta = 22.5°$ is much smaller than that for $\theta = 0°$, as shown in Figure 7. Clearly, smaller vibrations mean smaller output power. This phenomenon is more severe when wind direction $\theta = 45°$. As can be seen from Figure 7, the cylinder almost ceases to vibrate, and hence, the generated output power shown in Figure 6 is marginal. It can be concluded that further increasing wind direction after 45° results less structural vibrations and consequently hardly generate energy. Evidently, this kind of single-beam EH works efficiently only in a very narrow range of wind direction, which seriously limits the practical application of this type of harvester due to the uncertainty of wind direction in nature wind environment.

4.3 | Performance of the proposed omnidirectional EH

Although the two PESs in the proposed omnidirectional EH can generate electric energy simultaneously, it is worthwhile to first examine the output energy of each PES individually. Figure 8 shows the output power of the upper and lower PESs (P_1 and P_2) under different wind speeds and directions. As can be seen from Figure 8A, the output power of the upper PES for $\theta = 0°$ is close to that of the single-beam EH shown in Figure 6, which verifies the measurement accuracy of the proposed bibeam EH. Meanwhile, the output energy of the lower PES under this wind direction

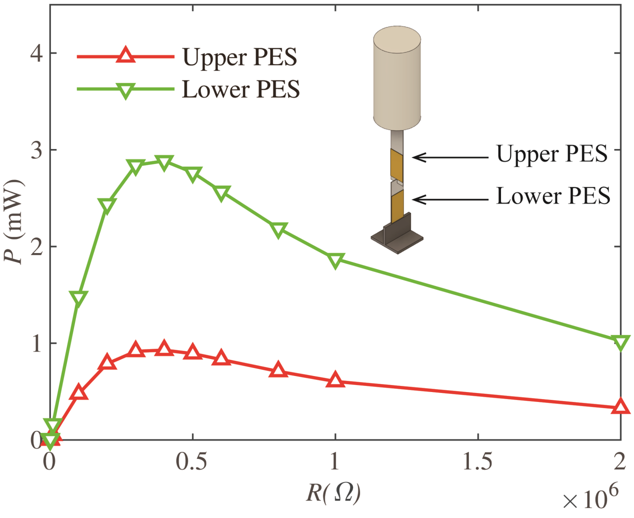

FIGURE 5 Variations of average output power with electrical load resistance for the bibeam piezoelectric wind EH

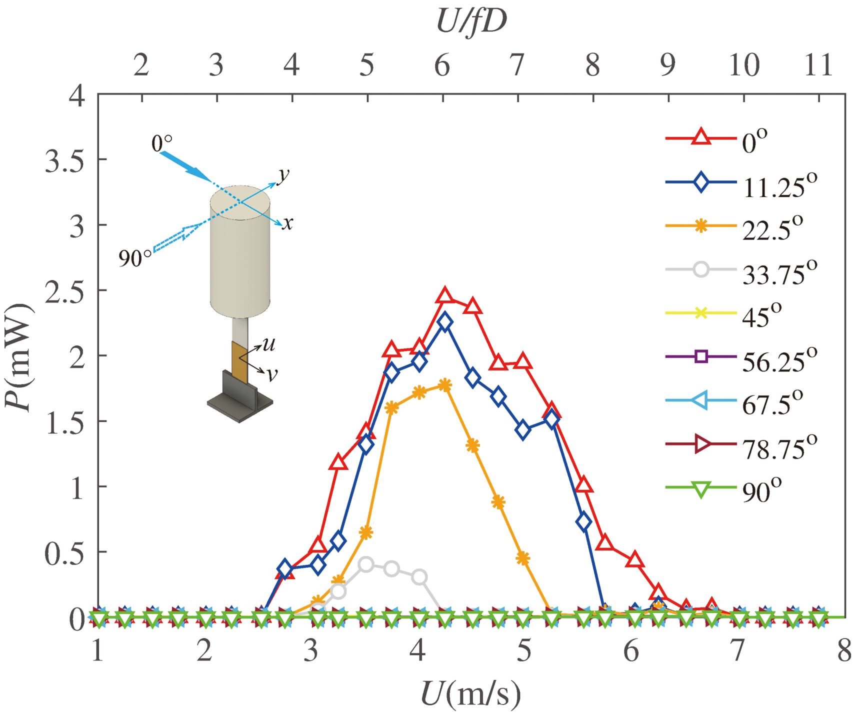

FIGURE 6 Average output power of the single-beam EH for different wind directions and speeds

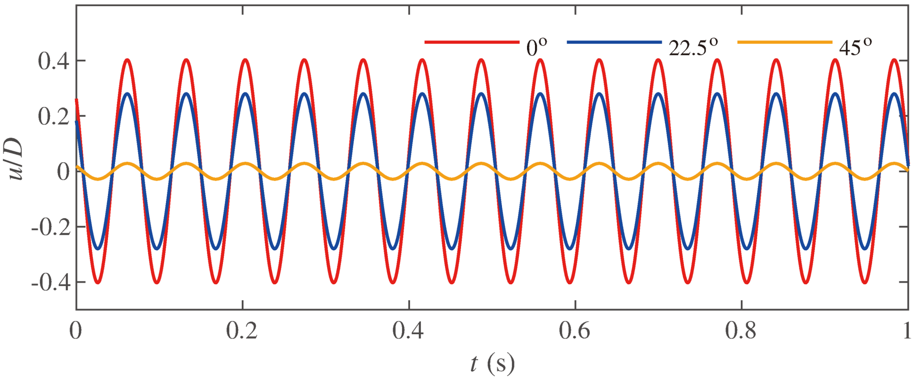

FIGURE 7 Time histories of the circular cylinder displacement responses for $\theta = 0°$, 22.5°, and 45°

is marginal, because when $\theta = 0°$ the along-wind vibration is negligible compared to the VIV in the cross-wind direction. When θ gradually increases from 11.25° to 22.5°, the output power of the upper PES of the bibeam EH still maintains a credible level when wind speed U is in the range of 4 to 5 m/s, as shown Figure 8A. In addition, the output power of the lower PES shown in Figure 8B is already considerable when $\theta = 45°$. The output power is higher than that of the upper PES due to higher bending deformation. The output power of the lower PES further increases after $\theta = 45°$, which can compensate the decrease in the power generated from the upper beam. This observation totally differs from that for the associated single-beam EH shown in Figure 6, where the output energy is already negligible when $\theta \geq 45°$. Furthermore, the range of working wind velocity of the bibeam EH shown in Figure 8A does not decrease significantly with increasing wind direction. For example, when $\theta = 45°$, the range of working wind velocity of the upper beam is still about 70% of that for $\theta = 0°$, indicating high efficiency and adaptability of the proposed EH.

Figure 9 shows the variation of the total output power P (i.e., $P = P_1 + P_2$) of the two PESs in the proposed bibeam wind EH, with wind direction and speed. A distinct finding from the figure is that the proposed bibeam wind EH exhibits high output energy and a wide range of effectively working speed for all wind directions from 0° to 90°. Comparing Figure 9 with Figure 6 clearly indicates that the performance of the wind EH has been improved significantly from a single wind direction EH to an omnidirectional wind EH.

The improvement of the proposed bibeam wind EH performance can be explained by the displacement responses at the top of the circular cylinder under different wind directions. As shown in Figure 10A,C, when wind direction $\theta = 22.5°$ or 33.75°, the displacement responses of the

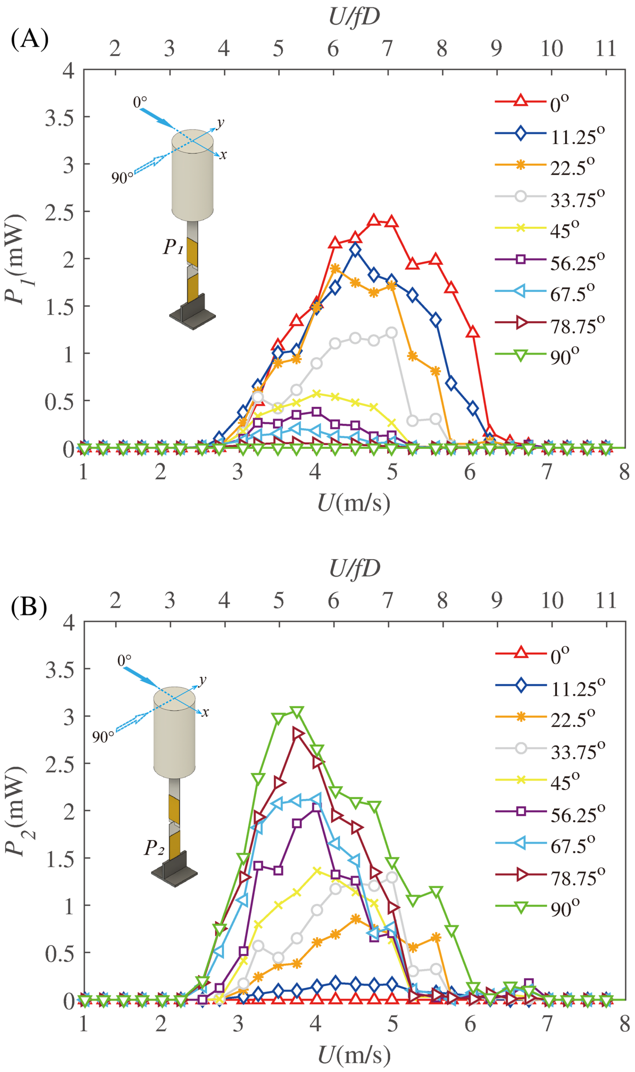

FIGURE 8 Average output power of the bibeam harvester from (A) upper piezoelectric sheet and (B) lower piezoelectric sheet

bibeam EH in direction *u* still keep a high level compared with those of single-beam EH (gray line in Figure 10). In addition, the displacement responses of the bibeam EH in directions *u* and *v* are rather harmonic, and the periods of the displacement responses in directions *u* and *v* are identical due to the same natural frequencies in these two directions. The resultant total displacement response (***u*** + ***v***), which is the summation of displacement response vectors of *u* and *v*, is found to be perpendicular to the approaching wind, as shown in Figure 10B,D. In other words, no matter what the wind direction is, the total vibrations of the circular cylinder of the bibeam EH are perpendicular to the approaching wind, which is just the reason that enables the proposed bibeam EH work effectively for θ = 22.5°. This can also be verified by the oscillation trajectories shown in Figure 11, which shows the trajectories of the top of the circular cylinder under different wind directions (shown in different rows) and different wind speed (shown in different columns). The maximum ratio of the displacement response in direction *y* to the diameter of the circular cylinder, that is, *y*/*D*, is shown in each subfigure for each case. The associated value of *x*/*D* is not shown in the figure due to the space limit but can be readily determined by using the two equal axes. As can be seen from Figure 11A, when wind direction = 0°, the vibration of the single-beam EH is perpendicular to the direction of the incoming flow. However, when θ changes from 0° to 45° (i.e., from the first row to the fifth row of Figure 11A), the dominant vibration direction of the single-beam EH is no longer perpendicular to the approaching wind direction. On one hand, the asymmetrical vibrations can interrupt the ideal periodic vortex shedding and hence decrease the lift force $F_{fluid,u}$ and the lock-in range. On the other hand, the projected component of the lift force along the vibration direction is smaller than that for θ = 0°. Therefore, the vibration of the single-beam EH for θ = 45° is already minimal and the resultant output energy decreases significantly. In sharp contrast, the dominant vibration of the bibeam EH in direction *y* (i.e., the cross-wind direction) does not decrease significantly when θ changes from 0° to 90° and *U* is around 4 m/s, as shown in the Figure 11B. The vibration trajectories are always perpendicular to the wind direction and parallel to the cross-wind vortex-induced force. The proposed bibeam EH vibrates in *u* and *v* directions concurrently. The cross-wind forces acting on the cylinder have the projected components along both the two vibration directions, *u* and *v*. The response components in these two directions then follow the same proportion, and hence, the summation of these two response vectors is along just the cross-wind direction *y* and perpendicular to the incoming flow. In other words, even for θ = 45°, the vibrations of the bibeam EH do not greatly attenuate the typical periodic vortex shedding, and hence,

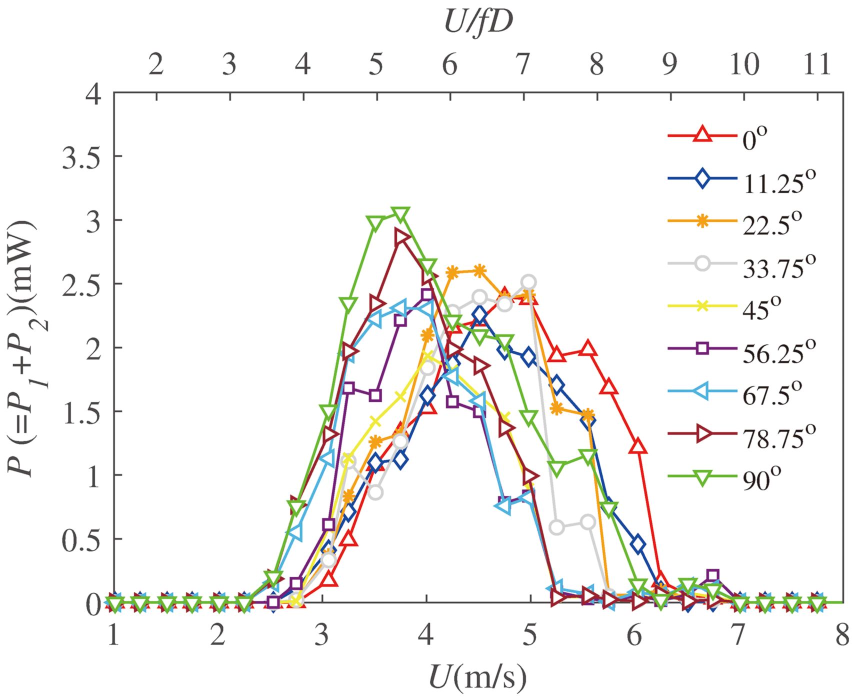

FIGURE 9 Variations of average total output power of the bibeam wind harvester with wind direction and speed

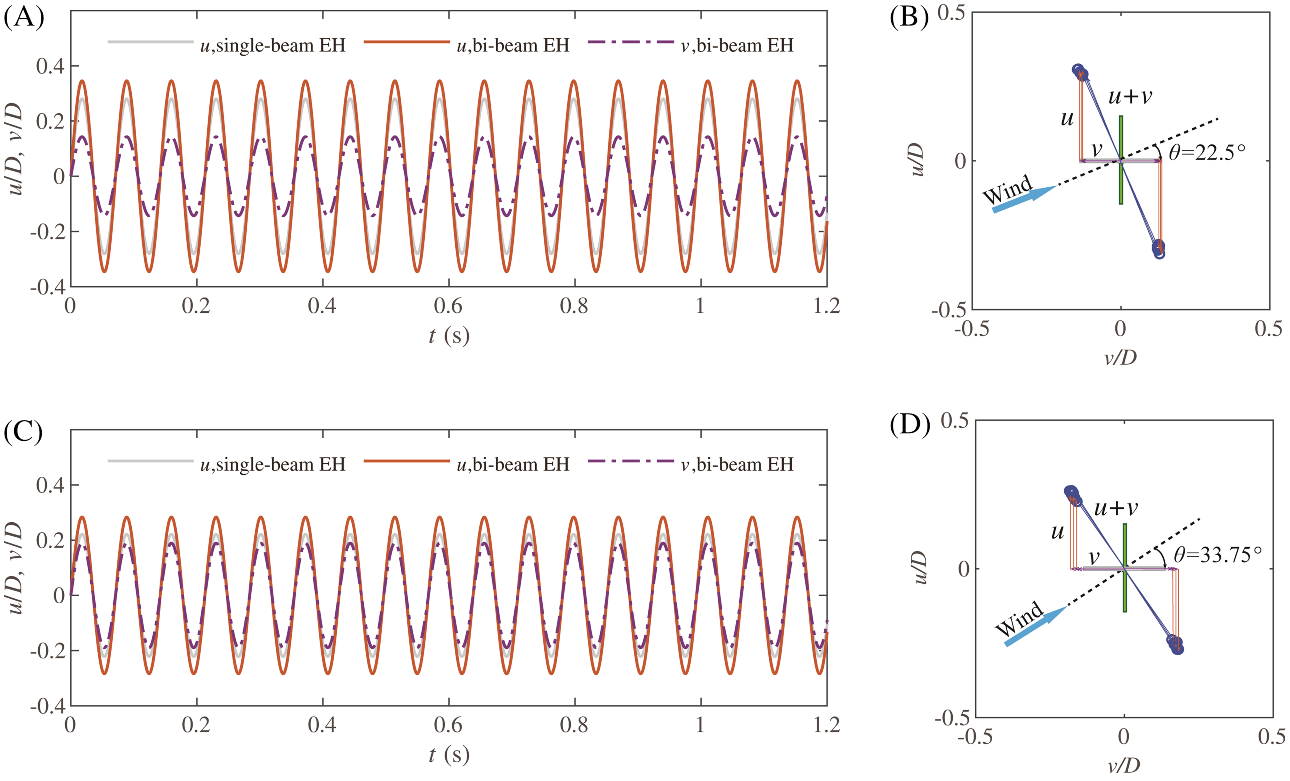

FIGURE 10 (A) Time histories of displacement responses of bibeam wind EH and single-beam wind EH for θ = 22.5°. (B) Vectors of displacement response components for θ = 22.5°. (C) Time histories of displacement responses of bibeam wind EH and single-beam wind EH for θ = 33.75°. (D) Vectors of displacement response components for θ = 33.75°

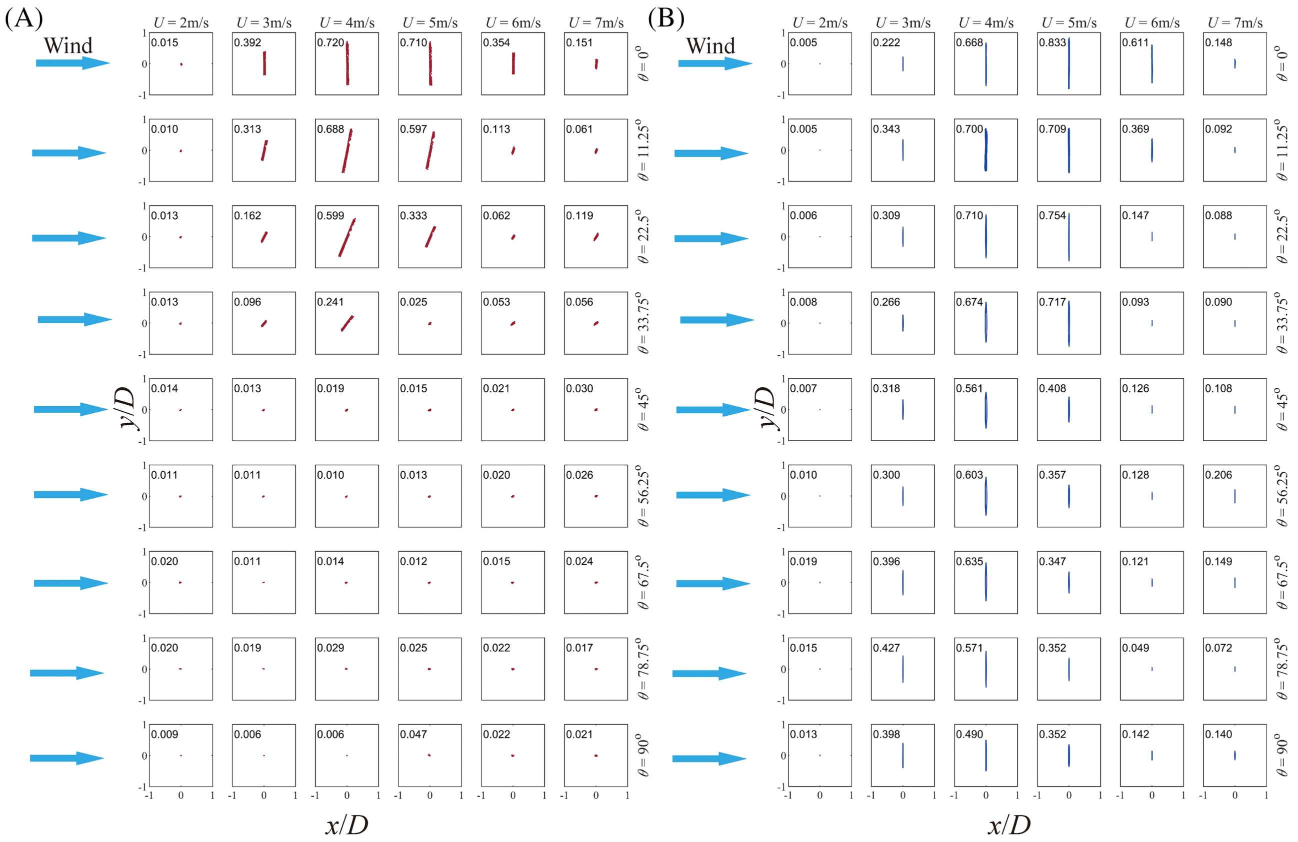

FIGURE 11 Oscillation trajectories of the top of circular cylinder under different wind directions and velocities for (A) the single-beam EH and (B) the proposed bibeam EH

the responses just exhibit a minor reduction compared to those for $\theta = 0°$. Therefore, when θ changes from 0° to 45°, the total output power P (i.e., $P = P_1 + P_2$) of the two PESs in the proposed bibeam EH only slightly decreases, as shown in Figure 9, which shows enormous advantages of the bibeam wind EH over that shown in Figure 6 for the traditional single-beam EH. When wind direction $\theta > 45°$, it can be observed from Figure 11B that the response components of the bibeam EH are much larger than that of the single-beam EH, when U is around 4 m/s. For the same reason discussed above, the resultant total displacement response ($\boldsymbol{u} + \boldsymbol{v}$) of the bibeam EH is still perpendicular to the approaching wind, and hence, the cross-wind responses are significant, and more importantly, far larger than those of the single-beam wind EH, as shown in Figure 11. Therefore, it can be concluded that for the rest of wind directions, the resultant total displacement responses of the bibeam EH are always perpendicular to the approaching wind, leading to considerable cross-wind responses and therefore significant total output power for all wind directions.

To emphasize the omnidirectional effectiveness of the bibeam wind EH, the maximum total output energy and the range of wind speed having enough power (say $P > 1$ mW) against all wind directions is shown in Figure 12. The power of microcontroller units and some environment sensors is in the order of milliwatts.[48] The 1-mW EH is able to power the ViPSN which is an Internet of Things (IoT) platform for the vibration-powered sensing and transmitting system.[49] In the figure, the results for $90° < \theta \leq 360°$ are determined by symmetry. As can be seen, the single-beam EH almost fails and cannot generate meaningful power except for wind directions around $\theta = 0°$ and 180°. In contrast, the performance of the bibeam EH remains considerable for all wind directions. All the maximum values of output energy for all the other wind directions are more than 80% of that for $\theta = 0°$, as shown in Figure 12A. Meanwhile, the wind speed that can generate power $P > 1$ mW covers a wide range for all wind directions, much wider than that of the single-beam EH, as shown in Figure 12B. All these observations clearly indicate the reliability and robustness of the proposed bibeam EH, which greatly enhances the efficiency and application range of VIV-based piezoelectric wind EHs in a natural wind environment.

5 | SUMMARY

This study has developed a VIV-based omnidirectional wind EH with an orthogonal bibeam system. Through wind tunnel experimental investigations, the following conclusions have been obtained.

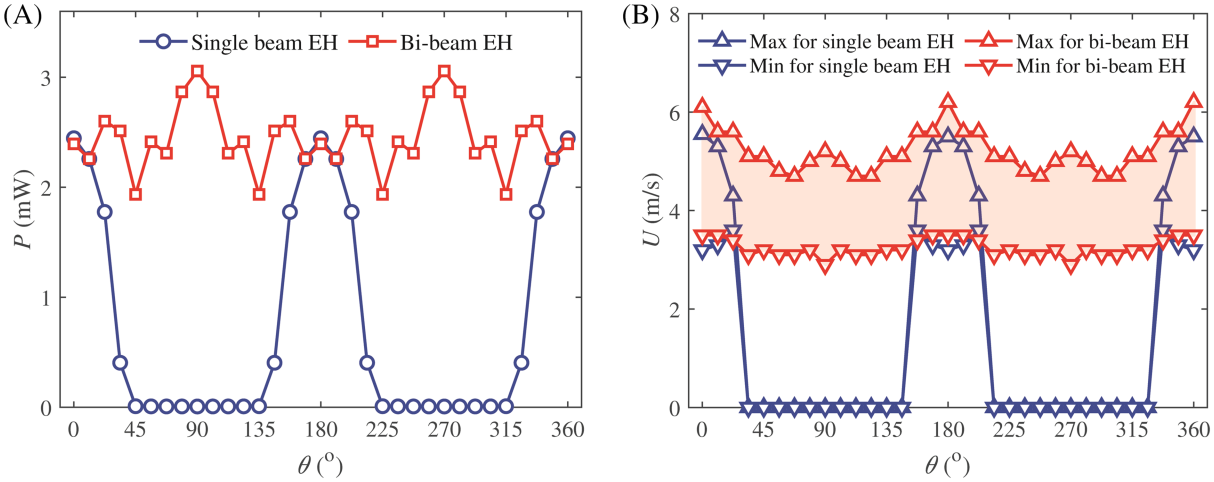

FIGURE 12 Variations of (A) maximal total output power and (B) effectively working wind velocity with wind direction

1. For the traditional single-beam wind energy, vortex shedding causes large amplitude vibrations and generated large output power for $\theta = 0°$. The harvester remains significant vibration and output for $0° < \theta \leq 22.5°$. When $22.5° < \theta \leq 90°$, the harvester ceases to vibrate, and hence, the generated output power is marginal.
2. The proposed bibeam wind EH exhibits high output energy and a wide range of effectively working speed for all wind directions, achieving the objective of an omnidirectional wind EH.
3. The underlying mechanism that makes the success of the proposed EH has been explained by the vibration trajectories of the harvester. With two degrees of freedom, the bibeam harvester is able to vibrate in the two directions simultaneously. The resultant total displacement responses of the bibeam EH are almost always perpendicular to the approaching wind, leading to considerable cross-wind responses and therefore significant total output power for all wind directions.
4. The performance of bibeam wind EH and single-beam wind EH has been compared. The proposed bibeam wind EH exhibits overwhelming advantages when the beam is skew to the incoming flow. For all wind directions, both the maximum output power and the range of operating wind speed of the bibeam wind EH are maintained at a high level, reinforcing the robustness of the proposed omnidirectional wind EH.

ACKNOWLEDGEMENTS

This work was supported by the National Natural Science Foundation of China under project No. 51478369 and No. 51608398 and Shenzhen Basic Research Program (JCYJ20170811160652645).

PEER REVIEW

The peer review history for this article is available at https://publons.com/publon/10.1002/we.2624.

ORCID

Jie Song https://orcid.org/0000-0001-6543-1053

REFERENCES

1. Shaikh FK, Zeadally S. Energy harvesting in wireless sensor networks: a comprehensive review. *Renew Sustain Energy Rev*. 2016;55:1041-1054.
2. Alaei E, Afrasiab H, Dardel M. Analytical and numerical fluid–structure interaction study of a microscale piezoelectric wind energy harvester. *Wind Energy*. 2020;23(6):1444-1460.
3. Larsen A. A generalized model for assessment of vortex-induced vibrations of flexible structures. *J Wind Eng Ind Aerodyn*. 1995;57(2):281-294.
4. Arunachalam S, Lakshmanan N. Across-wind response of tall circular chimneys to vortex shedding. *J Wind Eng Ind Aerodyn*. 2015;145:187-195.
5. Abdelkefi A, Hajj MR, Nayfeh AH. Phenomena and modeling of piezoelectric energy harvesting from freely oscillating cylinders. *Nonlinear Dyn*. 2012;70(2):1377-1388.
6. Dai H, Abdelkefi A, Wang L. Theoretical modeling and nonlinear analysis of piezoelectric energy harvesting from vortex-induced vibrations. *J Intell Mater Syst Struct*. 2014;25(14):1861-1874.
7. Hu G, Tse KT, Kwok KCS. Enhanced performance of wind energy harvester by aerodynamic treatment of a square prism. *Appl Phys Lett*. 2016;108(12):123901.
8. Hu G, Wang J, Su Z, Li G, Peng H, Kwok KCS. Performance evaluation of twin piezoelectric wind energy harvesters under mutual interference. *Appl Phys Lett*. 2019;115(7):073901.

9. Javed U, Abdelkefi A. Role of the galloping force and moment of inertia of inclined square cylinders on the performance of hybrid galloping energy harvesters. *Appl Energy*. 2018;231:259-276.
10. Zhao L, Yang Y. An impact-based broadband aeroelastic energy harvester for concurrent wind and base vibration energy harvesting. *Appl Energy*. 2018;212:233-243.
11. Abdelkefi A, Nayfeh AH, Hajj MR. Enhancement of power harvesting from piezoaeroelastic systems. *Nonlinear Dyn*. 2012;68(4):531-541.
12. Orrego S, Shoele K, Ruas A, et al. Harvesting ambient wind energy with an inverted piezoelectric flag. *Appl Energy*. 2017;194:212-222.
13. McCarthy JM, Watkins S, Deivasigamani A, John SJ, Coman F. An investigation of fluttering piezoelectric energy harvesters in off-axis and turbulent flows. *J Wind Eng Ind Aerodyn*. 2015;136:101-113.
14. Petrini F, Gkoumas K. Piezoelectric energy harvesting from vortex shedding and galloping induced vibrations inside HVAC ducts. *Energ Buildings*. 2018;158:371-383.
15. Shan X, Tian H, Cao H, Xie T. Enhancing performance of a piezoelectric energy harvester system for concurrent flutter and vortex-induced vibration. *Energies*. 2020;13(12):1-19.
16. Yang K, Su K, Wang J, Wang J, Yin K, Litak G. Piezoelectric wind energy harvesting subjected to the conjunction of vortex-induced vibration and galloping: comprehensive parametric study and optimization. *Smart Mater Struct*. 2020;29(7):075035.
17. Abdelkefi A. Aeroelastic energy harvesting: a review. *Int J Eng Sci*. 2016;100:112-135.
18. Li D, Wu Y, Da Ronch A, Xiang J. Energy harvesting by means of flow-induced vibrations on aerospace vehicles. *Prog Aeosp Sci*. 2016;86:28-62.
19. Rostami AB, Armandei M. Renewable energy harvesting by vortex-induced motions: review and benchmarking of technologies. *Renew Sustain Energy Rev*. 2017;70:193-214.
20. Wei C, Jing X. A comprehensive review on vibration energy harvesting: modelling and realization. *Renew Sustain Energy Rev*. 2017;74:1-18.
21. Zou H, Zhao L, Gao Q, et al. Mechanical modulations for enhancing energy harvesting: principles, methods and applications. *Appl Energy*. 2019;255:113871.
22. Watson S, Moro A, Reis V, et al. Future emerging technologies in the wind power sector: a European perspective. *Renew Sustain Energy Rev*. 2019;113:109270.
23. Chen W-L, Xin D-B, Xu F, Li H, Ou J-P, Hu H. Suppression of vortex-induced vibration of a circular cylinder using suction-based flow control. *J Fluids Struct*. 2013;42:25-39.
24. Chen W-L, Gao D-L, Yuan W-Y, Li H, Hu H. Passive jet control of flow around a circular cylinder. *Experiments in Fluids*. 2015;56(11):1-15.
25. Hu G, Kwok KCS. Predicting wind pressures around circular cylinders using machine learning techniques. *J Wind Eng Ind Aerodyn*. 2020;198:104099.
26. Bernitsas MM, Raghavan K, Ben-Simon Y, Garcia EMH. VIVACE (vortex induced vibration aquatic clean energy): a new concept in generation of clean and renewable energy from fluid flow. *J Offshore Mech Arct Eng*. 2008;130(4):1-15.
27. Akaydin HD, Elvin N, Andreopoulos Y. The performance of a self-excited fluidic energy harvester. *Smart Mater Struct*. 2012;21(2):025007.
28. Mehmood A, Abdelkefi A, Hajj MR, Nayfeh AH, Akhtar I, Nuhait AO. Piezoelectric energy harvesting from vortex-induced vibrations of circular cylinder. *J Sound Vibr*. 2013;332(19):4656-4667.
29. Abdelkefi A, Scanlon JM, McDowell E, Hajj MR. Performance enhancement of piezoelectric energy harvesters from wake galloping. *Appl Phys Lett*. 2013;103(3):033903.
30. Zhang LB, Dai HL, Abdelkefi A, Wang L. Improving the performance of aeroelastic energy harvesters by an interference cylinder. *Appl Phys Lett*. 2017;111(7):073904.
31. Zhang LB, Abdelkefi A, Dai HL, Naseer R, Wang L. Design and experimental analysis of broadband energy harvesting from vortex-induced vibrations. *J Sound Vibr*. 2017;408:210-219.
32. Naseer R, Dai HL, Abdelkefi A, Wang L. Piezomagnetoelastic energy harvesting from vortex-induced vibrations using monostable characteristics. *Appl Energy*. 2017;203:142-153.
33. Song J, Hu G, Tse KT, Li SW, Kwok KCS. Performance of a circular cylinder piezoelectric wind energy harvester fitted with a splitter plate. *Appl Phys Lett*. 2017;111(22):223903.
34. Hu G, Tse KT, Kwok KCS, Song J, Lyu Y. Aerodynamic modification to a circular cylinder to enhance the piezoelectric wind energy harvesting. *Appl Phys Lett*. 2016;109(19):193902.
35. Hu G, Tse KT, Wei M, Naseer R, Abdelkefi A, Kwok KCS. Experimental investigation on the efficiency of circular cylinder-based wind energy harvester with different rod-shaped attachments. *Appl Energy*. 2018;226:682-689.
36. Ding L, Yang L, Yang Z, Zhang L, Wu C, Yan B. Performance improvement of aeroelastic energy harvesters with two symmetrical fin-shaped rods. *J Wind Eng Ind Aerodyn*. 2020;196:104051.
37. Dai HL, Abdelkefi A, Wang L. Piezoelectric energy harvesting from concurrent vortex-induced vibrations and base excitations. *Nonlinear Dyn*. 2014;77(3):967-981.
38. Qin W, Deng W, Pan J, Zhou Z, Du W, Zhu P. Harvesting wind energy with bi-stable snap-through excited by vortex-induced vibration and galloping. *Energy*. 2019;189:116237.
39. Jubran BA, Hamdan MN, Al Bedoor BO. Roughness and turbulence intensity effects on the induced flow oscillation of a single cylinder. *Applied Scientific Research*. 1992;49(1):101-115.
40. Zhu J, Wang XQ, Xie W-C, So RMC. Turbulence effects on fluidelastic instability of a cylinder in a shear flow. *J Sound Vibr*. 2009;321(3):680-703.
41. Li D, Hong S, Gu S, et al. Polymer piezoelectric energy harvesters for low wind speed. *Appl Phys Lett*. 2014;104(1):012902.
42. Zhao J, Yang J, Lin Z, et al. An arc-shaped piezoelectric generator for multi-directional wind energy harvesting. *Sens Actuator A-Phys*. 2015;236:173-179.
43. Gong Y, Shan X, Luo X, Pan J, Xie T, Yang Z. Direction-adaptive energy harvesting with a guide wing under flow-induced oscillations. *Energy*. 2019;187:115983.
44. Atherton TJ, Kerbyson DJ. Size invariant circle detection. *Image Vision Comput*. 1999;17(11):795-803.
45. Ballard DH. Generalizing the Hough transform to detect arbitrary shapes. *Pattern Recognit*. 1981;13(2):111-122.
46. Li H, Chen W-L, Xu F, Li F-C, Ou J-P. A numerical and experimental hybrid approach for the investigation of aerodynamic forces on stay cables suffering from rain-wind induced vibration. *J Fluids Struct*. 2010;26(7):1195-1215.

47. Xu F, Chen W-L, Xiao Y-Q, Li H, Ou J-P. Numerical study on the suppression of the vortex-induced vibration of an elastically mounted cylinder by a traveling wave wall. *J Fluids Struct*. 2014;44:145-165.
48. Shah J, Mishra B. IoT-enabled low power environment monitoring system for prediction of PM2.5. *Pervasive Mob Comput*. 2020;67:101175.
49. Li X, Teng L, Tang H, et al. ViPSN: a vibration-powered IoT platform. *IEEE Internet Things J*. 2020;1-1.

How to cite this article: Shi T, Hu G, Zou L, Song J, Kwok KCS. Performance of an omnidirectional piezoelectric wind energy harvester. *Wind Energy*. 2021;24(11):1167-1179. https://doi.org/10.1002/we.2624